

## Structural, electrical and optical studies on spray-deposited aluminium-doped ZnO thin films

S TEWARI<sup>1</sup> and A BHATTACHARJEE<sup>2,\*</sup>

<sup>1</sup>Department of Physics, Karimganj College, Karimganj 780 710, India

<sup>2</sup>Department of Physics, National Institute of Technology, Silchar 788 010, India

\*Corresponding author. E-mail: ayonbh@gmail.com

MS received 5 November 2009; revised 12 June 2010; accepted 17 June 2010

**Abstract.** Thin films of zinc oxide (ZnO) were deposited on cleaned glass substrates by chemical spray pyrolysis technique using  $\text{Zn}(\text{CH}_3\text{COO})_2$  as precursor solution. Also, aluminium-doped thin films of ZnO were prepared by using  $\text{AlCl}_3$  as doping solution for aluminium. The dopant concentration [Al/Zn atomic percentage (at%)] was varied from 0 to 1.5 at% in thin films of ZnO prepared in different depositions. Structural characterization of the deposited films was performed with X-ray diffraction (XRD) studies. It confirmed that all the films were of zinc oxide having polycrystalline nature and possessing typical hexagonal wurtzite structure with crystallite size varying between 100.7 and 268.6 nm. The films exhibited changes in relative intensities and crystallite size with changes in the doping concentration of Al. The electrical studies established that 1 at% of Al-doping was the optimum for enhancing electrical conduction in ZnO thin films and beyond that the distortion caused in the lattice lowered the conductivity. The films also exhibited distinct changes in their optical properties at different doping concentrations, including a blue shift and slight widening of bandgap with increasing Al dopant concentration.

**Keywords.** Zinc oxide thin films; Al-doping; spray pyrolysis; electrical properties; optical properties; structural properties.

**PACS Nos** 68.55.-a; 73.50.-h; 78.20.-e; 77.55.hf

### 1. Introduction

Zinc oxide (ZnO) is one of the most prominent metal oxide semiconductors. It is an n-type semiconductor of hexagonal (wurtzite) structure with a direct energy wide bandgap of about 3.37 eV at room temperature [1]. It is a versatile material with good electrical and optical properties, thermal and chemical stability, is abundant in nature, low-cost and non-toxic. Due to this versatility ZnO has drawn considerable attention and has been investigated in various forms such as single crystals, sintered pellets, thick films, nanobelts and thin films [2–14]. The thin films of ZnO find a multitude of immensely important

applications in electronic and optoelectronic devices such as transparent conductors, solar cell windows, gas sensors, surface acoustic wave (SAW) devices, heat mirrors etc. [2–10]. It is also being considered as a potential candidate in the new frontiers of research like spintronics [11].

The performance and efficiency of thin film-based devices are determined strongly by the structural, electrical and optical properties of the component films. A study of these properties and their dependence on the film characteristics is very important as it helps in optimizing film parameters for better device applications. Further, the electrical and optical properties of the thin films are determined by the process parameters during film growth such as flow-rate, substrate temperature, concentration of the solution etc., as well as by the presence of impurities and defects in the films. For transparent conducting oxide (TCO) thin films like ZnO, it is always desired to improve the electrical conduction without affecting its excellent optical properties. Also, on doping the properties of ZnO thin films have shown some interesting features; e.g. Mn-doped ZnO thin films behave as diluted magnetic semiconductors and has promising potential in spintronics [11,12]. As such, it is very important to optimize the process parameters of film growth and doping levels to have a desired enhanced device performance. Al is chosen as dopant material because of its easy and abundant availability and also, because it enhances the gas-sensing properties of the ZnO thin films, which has immensely important industrial and domestic applications for detecting hazardous gases, including LPG [13,14].

## **2. Experimental procedure**

The films of ZnO were deposited on glass substrates by chemical spray pyrolysis technique. It is a very simple and relatively cost-effective method for preparing films of any desired composition under controlled conditions, involving the spraying of a solution containing a soluble salt of the cation of interest onto a heated substrate. The details of film deposition has been reported elsewhere [15,16]. In the present investigation the ZnO thin films were deposited on properly cleaned glass substrates, all having  $2.5 \text{ cm} \times 1 \text{ cm}$  dimension. The precursor solution used was of 0.1 M concentration of high purity zinc acetate dehydrate (Merck, India) prepared in distilled water. Aluminium chloride (Merck, India) was used as the source of dopant. The dopant concentration of aluminium (Al/Zn at%) was varied from 0 to 1.5 at% in different depositions. All the undoped and Al-doped ZnO thin films of three different doping concentrations were prepared separately in different depositions under the same parametric conditions, as given in table 1.

The detailed description of the spray system is given in [15]. During optimization of the process parameters for preparing ZnO thin films, the substrate temperature was found to be the most important parameter influencing the film properties. To obtain good-quality ZnO thin films, suitable for gas-sensing studies, the optimized value of substrate temperature was found to be  $410^\circ\text{C}$ , which we have reported previously [16]. In the present investigation the substrate temperature was therefore kept at a constant value of  $(410 \pm 10)^\circ\text{C}$ . Film thickness was determined by the weight-difference method using an electronic high-precision balance (Citizen, Model: CY 204) and was confirmed again using Tollensky's interference method. All the film thicknesses were found to be in the

**Table 1.** Spray parameters for film deposition.

Spray parameter	Value
Concentration of zinc acetate solution	0.1 M
Nozzle–substrate distance	50 cm
Solution flow rate	5 ml/min
Gas pressure	3 kg/cm <sup>2</sup>
Substrate temperature	410 ± 10°C

range 250–310 nm. The temperature was monitored during the entire deposition process using a pre-calibrated chromel-alumel thermocouple with the help of Motwane digital multimeter (Model: 545)

The structural characterization of the films was performed using grazing incidence X-ray diffraction (GIXRD) analysis for phase identification using PANalytical X'Pert Pro X-ray Diffractometer with Cu-K $\alpha$  radiation ( $\lambda = 1.5418 \text{ \AA}$ ) X-ray source at 40 kV and 30 mA in the scanning angle ( $2\theta$ ) from 30° to 70° with a scan speed of 0.001°/s.

For electrical characterization, high conducting silver paste was used to make ohmic contacts on both ends of the ZnO thin films. The contacts were properly heated and allowed to dry. The films were mounted on a two-probe assembly kept inside a silica tube which was inserted coaxially inside a tubular furnace. The temperature of the film was varied from room temperature (20°C) to 400°C in steps and allowed to equilibrate for some time at intervals of 10°C. At each stable temperature, the electrical resistivity of the film was obtained from the resistance measurements performed using a Keithley System Electrometer (Model: 6514)

The optical transmission spectra for undoped and Al-doped ZnO thin films were obtained in the ultraviolet (UV)/visible/near-infrared (NIR) region from 200 to 1100 nm using Perkin Elmer UV-VIS spectrophotometer (Model: Lambda 35). The measurements were carried out in the wavelength scanning mode for normal incidence at room temperature using an uncoated glass slide as reference.

### 3. Results and discussion

#### 3.1 Structural studies

Figure 1 shows the X-ray diffraction (XRD) patterns of the undoped and Al-doped ZnO films. Using X'Pert High Score software, the observed XRD pattern is found to match with the ICDD Reference Pattern: zinc oxide, 01-070-8072. It is observed that all the films are polycrystalline in nature, possessing hexagonal wurtzite structure. No phase corresponding to aluminium or other aluminium compounds was observed in the GIXRD patterns. The most prominent peak observed in the undoped film corresponded to (1 0 1) plane. Other peaks corresponding to (1 0 0), (0 0 2), (1 0 2), (1 0 3), (1 1 2), (1 0 4) etc.

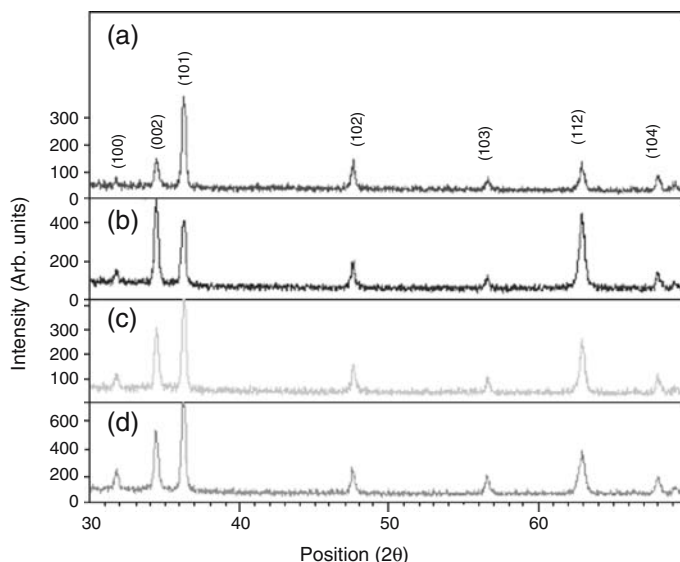


**Figure 1.** GIXRD pattern of ZnO thin films: (a) Undoped ZnO thin films, (b) 0.5 at% Al-doped ZnO thin films, (c) 1 at% Al-doped ZnO thin films and (d) 1.5 at% Al-doped ZnO thin films.

were observed with low relative intensities with (100) being the lowest. On doping the ZnO films by 0.5 at% Al, the intensity of the peaks corresponding to (100), (002) and (112) improved, however, the most intense peak corresponded to (002) plane. Other peaks corresponding to (101), (102), (103) and (104) planes were also present with relatively lower intensities.

On further increase of Al-dopant concentration, the intensity of the peak corresponding to (101) reflection plane keeps on improving and again became most intense for 1 at% Al in this study. With increasing Al-dopant concentration, the positions of the measured peaks do not change significantly but the intensity of (002) and (112) peaks improve drastically in 0.5 at% and 1 at%, however it decreases slightly after that. However, the intensity of the peak (100) increases slowly throughout with increase in doping concentration. Similar results of change in preferential orientation had earlier been reported for Zr-doped ZnO films prepared by sol-gel method and Ga-doped ZnO films prepared by spray pyrolysis [17,18].

The crystallite size  $D$  is calculated using the Scherrer formula [19]

$$D = \frac{k\lambda}{\beta \cos \theta}, \quad (1)$$

where  $k$  is a constant and in our case  $k = 0.9$ ,  $\lambda$  is the wavelength of the incident X-ray ( $\lambda = 1.5418 \text{ \AA}$ ),  $\beta$  is the corrected FWHM for instrumental broadening of the maximum intensity peak and  $\theta$  is the angle at which the maximum peak occurs.

The crystallite size of ZnO calculated for the most prominent peak with Al-dopant concentration is shown in table 2. It is observed that compared to undoped ZnO film, the crystallite size in the Al-doped films decreases. This is attributed to the replacement of relatively bigger  $Zn^{2+}$  ions by the relatively smaller  $Al^{3+}$  ions during the formation of the Al-doped ZnO films. As the radius of  $Al^{3+}$  ion is smaller than that of  $Zn^{2+}$  ion ( $r_{Al^{3+}} = 0.054$  nm and  $r_{Zn^{2+}} = 0.074$  nm), it leads to a decrease in the lattice constants, which in turn is responsible for the changes in the crystallite size. The minimum crystallite size of 103 nm is found for 0.5 at% Al-doped film. However, it is observed that the crystallite size in the doped films does not vary in any regular pattern with Al-dopant concentration, which is attributed to the lattice disorder produced in the films at higher dopant concentration due to difference in the ionic radii of  $Zn^{2+}$  and  $Al^{3+}$ .

### 3.2 Electrical studies

The variation of the resistivity of the ZnO thin film with temperature for the undoped and Al-doped ZnO thin films is shown in figure 2. It is evident from figure 2 that the resistivity of ZnO films decreases due to doping with Al by 0.5 at% and 1 at% but it almost returns to its undoped behaviour when the doping level is increased to 1.5 at%. The decrease in resistivity at 0.5 at% and 1 at% Al-dopant concentration is attributed to the replacement of  $Zn^{2+}$  by  $Al^{3+}$  ions which introduces a large number of electrons in the doped films, thereby increasing the number of charge carriers. Thus, the conductivity of the film increases. However, with further increase in doping concentration at 1.5 at%, sufficient disorder is produced in the lattice due to differences in the ionic radii of  $Zn^{2+}$  and  $Al^{3+}$ . This increases the efficiency of scattering mechanism such as phonon scattering and ionized impurity scattering which, in turn, causes the increase in resistivity. Moreover, neutral defects may be created which may be more pronounced at higher Al-dopant concentrations. So they neutralize the excess of charge carriers obtained with increased doping concentration which may be responsible for the increased resistivity. Another observation is that without Al-doping the resistivity of the ZnO thin film increases with temperature ranging from 80 to 150°C but the resistivity totally disappears in all the doped films.

Further, it is observed from the experiments that, the resistivity of the undoped film first increases with temperature up to about 150°C and beyond that follows the same trend as exhibited by the doped films. All the doped films exhibit nearly the four-region behaviour

**Table 2.** Structural properties of the undoped and Al-doped films.

Sample	Crystallite size (nm) calculated for the most prominent peak
Undoped (0 at% Al) ZnO film	278.6
0.5 at% Al-doped ZnO film	102.7
1 at% Al-doped ZnO film	261.2
1.5 at% Al-doped ZnO film	206.4

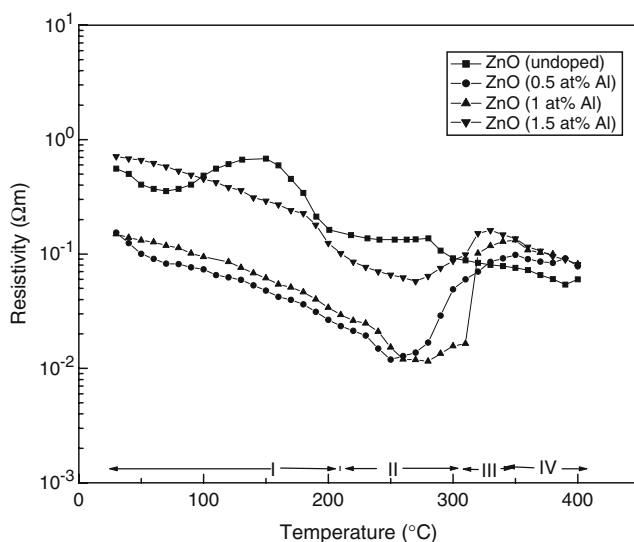


**Figure 2.** Resistivity variance with temperature for undoped ZnO and Al-doped ZnO thin films.

similar to that already reported [20]. However, in our study three regions are very distinctly found, with very thin third (III) region. In region I (20–225°C), the decrease in resistivity is attributed more to the thermal excitation of electrons into the conduction band. The sharp increase in resistivity in region II (225–325°C) is related to the vigorous oxygen adsorption on the film surface, causing decrease in the carrier concentration, which is consistent with the adsorption of oxygen on the surface of polycrystalline ZnO films as reported by other researchers [21,22]. At lower temperatures, the surface reactions proceed too slowly to be useful. However, as temperature increases, more number of oxygen moieties ( $O^{2-}$ ,  $O_2^-$ ,  $O^-$ ) are absorbed on the zinc oxide surface depending on temperature [16].

In region III (325–350°C), the resistivity is not much affected by the temperature change probably due to the equilibrium achieved between the two competing processes of thermal excitation of electrons and oxygen adsorption. Finally, the resistivity in region IV (350–400°C) decreases again which is attributed to the dominant thermal excitation of electrons and desorption of oxygen species. It may also be related to the increase in carrier concentration resulting from the activation of deep donors which may have arisen due to native defects such as interstitial zinc atoms and oxygen vacancies [23].

Since thermal excitation is the main cause of increase in electrical conductivity in regions I and IV, we calculated the thermal activation energies in these regions, from the plots of  $\ln \sigma$  vs.  $1000/T$  in figure 3. The thermal activation energies are listed in table 3.

The study indicates that with Al doping the films behaves differently in different temperature ranges. In region I (20–225°C), the thermal activation energy first decreases due to increase in the carrier concentrations up to 1 at% of Al doping. Beyond that the disturbances in the lattice due to increased number of Al species in Zn leads to increased

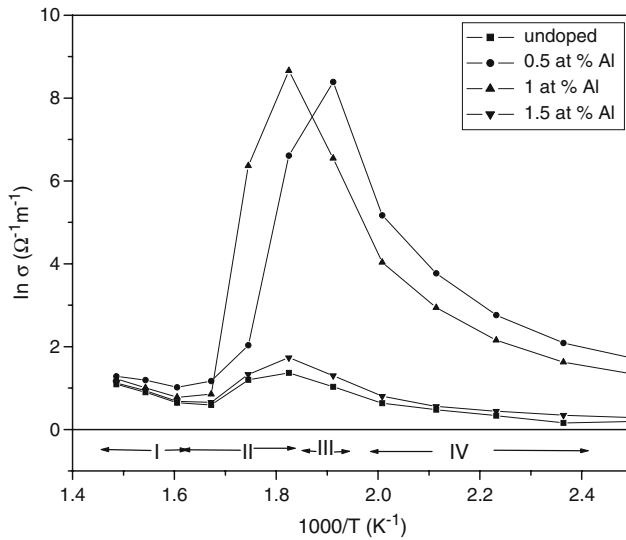


**Figure 3.** Variation of  $\ln \sigma (\Omega^{-1}m^{-1})$  vs.  $1000/T (K^{-1})$ .

thermal activation energy. However, in region IV (350–400°C), the value of the thermal activation keeps on increasing at all doping concentrations which increases the scattering phenomena such as phonon scattering and ionized impurity scattering with increased doping concentrations.

### 3.3 Optical studies

All the films show higher transmission for wavelengths longer than 400 nm (figure 4a). With increase in Al-doping the spectra show an increase in transmission near the fundamental absorption and in the UV region. A blue-shift of the absorption tail towards shorter wavelengths for higher Al-doping concentration and an enhanced transmission in UV region is observed in figure 4b. This blue-shift of the absorption edge of Al-doped

**Table 3.** Thermal activation energies for undoped and doped ZnO thin films.

Sample	Activation energy in region I $E_1$ (eV)	Activation energy in region IV $E_2$ (eV)
Undoped ZnO film	0.260	0.054
ZnO film (0.5 at% Al)	0.122	0.090
ZnO film (1 at% Al)	0.058	0.185
ZnO film (1.5 at% Al)	0.109	0.264

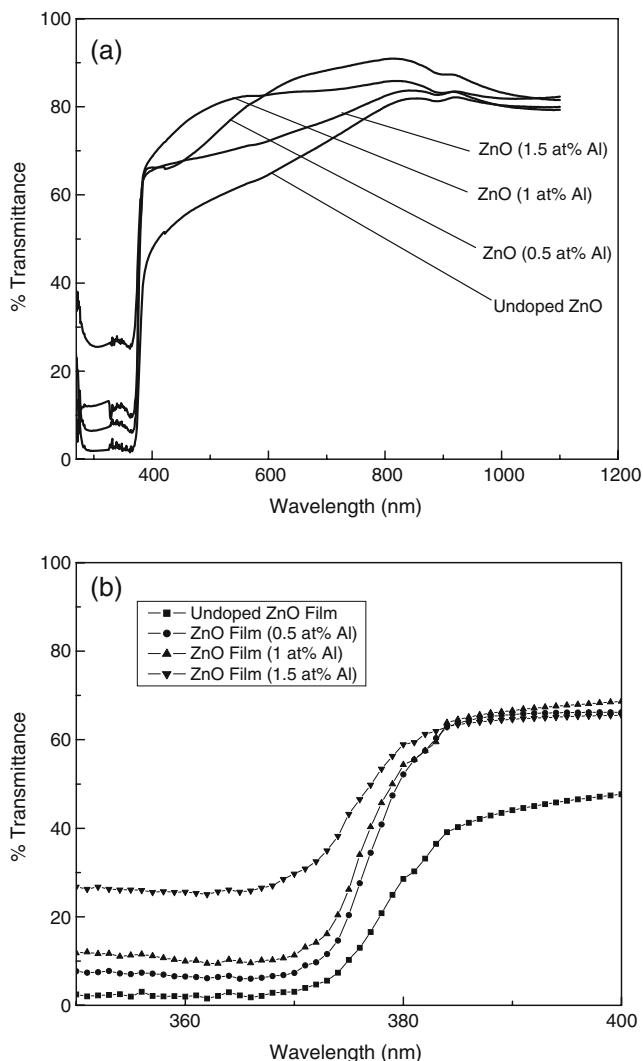


**Figure 4.** (a) Transmission spectra of the undoped and Al-doped ZnO thin films for varying Al-doping concentrations. (b) Blue-shift observed in the absorption edge of the transmittance pattern.

nanocrystalline films is attributed to the poor crystallinity of the films and also to increase in disorder with Al doping [24]. There have been reports of this kind of blue-shift, explained in terms of Burstein–Moss effect [25,26], according to which increase of the carrier concentration due to Al doping results in a shift of the Fermi level and block some of the lowest states, thereby causing widening of the bandgap resulting in the blue-shift of the absorption tail. This widening of the bandgap is also responsible for the enhanced transmission in the UV region.

*Structural, electrical and optical studies on spray-deposited ZnO*

The absorbance spectra of the undoped and Al-doped ZnO thin films having varying thicknesses are shown in figure 5. These spectra reveal that films grown under the same parametric conditions have low absorbance in the entire range. From the absorbance data, the absorption coefficient  $\alpha$  can be calculated using Lambert law [27]

$$\ln(I_0/I) = 2.303A = \alpha d, \quad (2)$$

where  $I_0$  and  $I$  are the intensity of incident and transmitted light respectively,  $A$  is the optical absorbance and  $d$  is the film thickness.

The absorption coefficient  $\alpha$  was found to follow the Tauc relation [28],

$$\alpha = [A_0(h\nu - E_g)^n]/h\nu, \quad (3)$$

where  $A_0$  is a constant which is related to the effective masses associated with the bands and  $E_g$  is the bandgap energy,  $h\nu$  is the photon energy,  $\alpha$  is the absorption coefficient,  $n$  is a constant which is 1/2 for direct bandgap material and  $n$  is 2 for indirect bandgap material. As our material was direct bandgap,

$$\alpha = [A_0(h\nu - E_g)^{1/2}]/h\nu \quad (4)$$

the extrapolation of straight line to  $ah\nu = 0$  axis gives the value of energy of bandgap.

Plots of  $(ah\nu)^2$  vs. the photon energy  $h\nu$  for films of varying doping concentrations are shown in figure 6.

Linearity of the plots indicates that the material is of direct bandgap nature. Extrapolation of linear portion of the graph to the energy axis at  $\alpha = 0$  gives the bandgap energy  $E_g = 3.1$  eV for the undoped film, further it is found to get wider with increasing Al-doping concentration up to 3.25 eV for 1.5 at% Al-doped ZnO thin films. This widening of the bandgap with doping concentration is consistent with the observation of blue-shift in the absorption tail of the transmittance spectra.

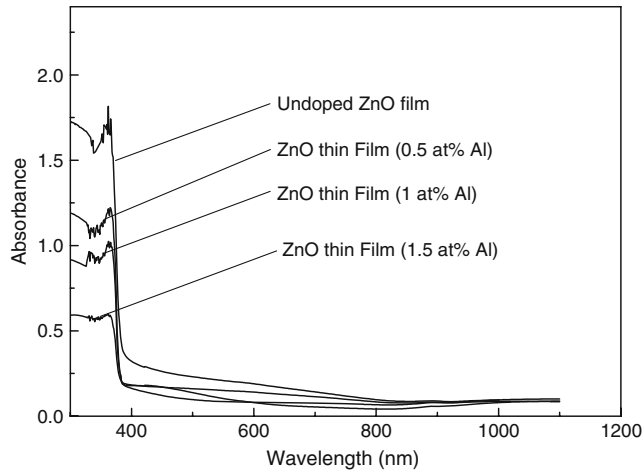


**Figure 5.** Absorbance spectra of the undoped and Al-doped ZnO thin films.

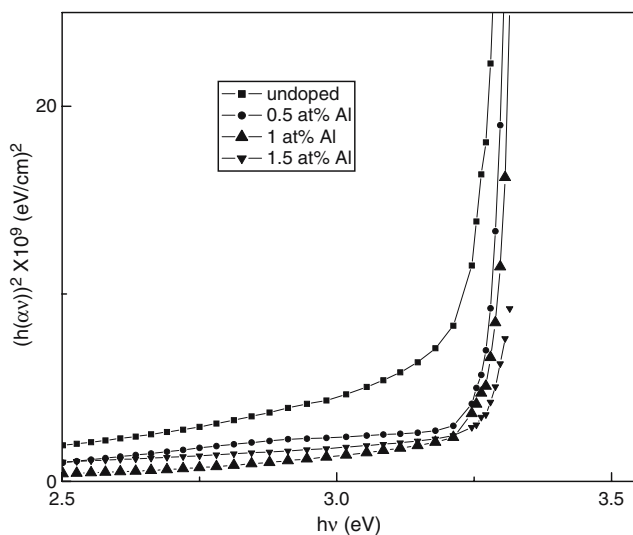


Figure 6. Plots of  $(\alpha hv)^2$  vs. the photon energy  $hv$ .

#### 4. Conclusion

The electrical and structural properties of Al-doped zinc oxide thin films prepared by the chemical spray pyrolysis was studied in this paper. The structural analysis confirmed the prepared films to be ZnO. Our studies revealed that there was a slight change in crystallite size which occurred with increasing doping concentration of Al. The electrical investigation revealed that with Al-doping the conductivity of the ZnO film initially improved upto 1 at% of Al-doping concentration, but beyond that it decreased with Al-doping (1.5 at%). The optical observations on the films indicate a blue-shift in the absorption edge, improved emission in the UV region and a widening of the bandgap with increasing Al-dopant concentration.

#### References

- [1] A Mang, K Reimann and St Rubenacke, *Solid State Commun.* **94**, 251 (1995)
- [2] K L Chopra, S Major and D R Pandya, *Thin Solid Films* **102**, 1 (1983)
- [3] K Elmer, *J. Phys. D: Appl. Phys.* **33**, R17 (2000)
- [4] M Krunk and E Mellikov, *Thin Solid Films* **270**, 33 (1995)
- [5] J A Aranovich, D Golmaya, A L Fahrenbruch and R H Bube, *J. Appl. Phys.* **51**, 4260 (1980)
- [6] P P Sahay, *J. Mater. Sci.* **40**, 4383 (2005)
- [7] H Nanto, T Minami and S Takata, *J. Appl. Phys.* **60**, 482 (1986)
- [8] K Arshak, I Gaiden, *Mater. Sci. Engg.* **B118**, 44 (2005)
- [9] Y Nakanishi, A Miyake, H Kominami, T Aoki, Y Hatanaka and G Shimaoka, *Appl. Surf. Sci.* **142**, 233 (1999)
- [10] R Ghosh, S Fujihara and D Basak, *J. Electron. Mater.* **35**, 9, 1728 (2006)

*Structural, electrical and optical studies on spray-deposited ZnO*

- [11] C Ronning, P X Gao, Y Ding, Z L Wang and D Schwen, *Appl. Phys. Lett.* **84**, 783 (2004)
- [12] L Yan, C K Ong and X S Rao, *J. Appl. Phys.* **96**, 508 (2004)
- [13] F Paraguay, D M Miki-Yoshida, J Morales, J Solis and W Estrada, *Thin Solid Films* **373**, 137 (2000)
- [14] B Baruwati, D K Kumar and S V Manorama, *Sens. Actuators* **B119**, 676 (2006)
- [15] P P Sahay, S Tewari and R K Nath, *Cryst. Res. Technol.* **42**, 723 (2007)
- [16] P P Sahay, S Tewari, S Jha, and M Shamsuddin, *J. Mater. Sci.* **40**, 4791 (2005)
- [17] G K Paul, S Bandyopadhyay, S K Sen and S Sen, *Mater. Chem. Phys.* **79**, 71 (2003)
- [18] A Tiburcio-Silver, A Sanchez-Juarez and A Avila-Garcia, *Sol. Energy Mater. Sol. Cells* **55**, 3 (1998)
- [19] H P Klug and L E Alexander, *X-ray diffraction procedures for polycrystalline and amorphous materials* (Wiley, New York, 1974)
- [20] C H Kwon, H-K Hong, D H Yun, K Lee, S-T Kim, Y-H Roh and B-H Lee, *Sens. Actuators* **B24**, 610 (1995)
- [21] J C Sen, *J. Vac. Sci. Technol.* **12**, 47 (1975)
- [22] N L Kenigsberg and A N Chernets, *Sov. Phys. Solid State* **10**, 2235 (1969)
- [23] F A Kroger, in: *The chemistry of imperfect crystals* (North-Holland, Amsterdam, 1964) p. 691
- [24] S T Tan, B J Chen, X W Sun and W J Fan, *J. Appl. Phys.* **98**, 013505 (2005)
- [25] E Burstein, *Phys Rev.* **93**, 632 (1954)
- [26] T S Moss, *Proc. Phys. Soc. London Ser.* **B67**, 775 (1954)
- [27] A Adachi, A Kudo and T Sakata, *Bull. Chem. Soc. Jpn.* **68**, 3283 (1995)
- [28] J I Pankove, *Optical processes in semiconductors* (Prentice-Hall, Englewood Cliffs, NJ, 1971)